Mon. Not. R. Astron. Soc. **337,** 1043–1058 (2002)

Near- and mid-infrared colours of star-forming galaxies in European Large Area *ISO* Survey fields

P. Väisänen,[1,2★] T. Morel,[3,4,5] M. Rowan-Robinson,[3] S. Serjeant,[3] S. Oliver,[3,6] T. Sumner,[3] H. Crockett,[3] C. Gruppioni[7,8] and E. V. Tollestrup[9,10]

[1]*Observatory, PO Box 14, University of Helsinki, Finland*
[2]*European Southern Observatory, Alonso de Cordova 3107, Vitacura, Casilla 19001, Santiago 19, Chile*
[3]*Astrophysics Group, Blackett Laboratory, Imperial College of Science, Technology & Medicine, Prince Consort Road, London SW7 2BZ*
[4]*IUCAA, Post Bag 4, Ganeshkhind, Pune 411 007, India*
[5]*Osservatorio Astronomico di Palermo, Piazza del Parlamento 1, 90134 Palermo, Italy*
[6]*Astronomy Centre, Physics and Astronomy Subject Group, School of CPES, University of Sussex, Falmer, Brighton BN1 9QJ*
[7]*Osservatorio Astronomico di Padova, Vicolo dell'Osservatorio 5, 35122 Padova, Italy*
[8]*Osservatorio Astronomico di Bologna, via Ranzani 1, 40127 Bologna, Italy*
[9]*Boston University, Department of Astronomy, 725 Commonwealth Avenue, Boston, MA 02215, USA*
[10]*Harvard–Smithsonian Center for Astrophysics, 60 Garden Street, Cambridge, MA 02138, USA*

Accepted 2002 August 16. Received 2002 February 4; in original form 2001 May 30

ABSTRACT

We present *J*- and *K*-band near-infrared (near-IR) photometry of a sample of mid-infrared (mid-IR) sources detected by the *Infrared Space Observatory* (*ISO*) as part of the European Large Area *ISO* Survey (ELAIS) and study their classification and star-forming properties. We have used the Preliminary ELAIS Catalogue for the 6.7-μm (LW2) and 15-μm (LW3) fluxes. All of the high-reliability LW2 sources and 80 per cent of the LW3 sources are identified in the near-IR survey reaching $K \approx 17.5$ mag. The near-IR/mid-IR flux ratios can effectively be used to separate stars from galaxies in mid-IR surveys. The stars detected in our survey region are used to derive a new accurate calibration for the ELAIS ISOCAM data in both the LW2 and LW3 filters. We show that near- to mid-IR colour–colour diagrams can be used to classify galaxies further, as well as to study star formation. The ELAIS ISOCAM survey is found mostly to detect strongly star-forming late-type galaxies, possibly starburst-powered galaxies, and it also picks out obscured active galactic nuclei. The ELAIS galaxies yield an average mid-IR flux ratio LW2/LW3 $= 0.67 \pm 0.27$. We discuss the $f_\nu(6.7\,\mu\mathrm{m})/f_\nu(15\,\mu\mathrm{m})$ ratio as a star formation tracer using *ISO* and *IRAS* data of a local comparison sample. We find that the $f_\nu(2.2\,\mu\mathrm{m})/f_\nu(15\,\mu\mathrm{m})$ ratio is also a good indicator of activity level in galaxies and conclude that the drop in the $f_\nu(6.7\,\mu\mathrm{m})/f_\nu(15\,\mu\mathrm{m})$ ratio seen in strongly star-forming galaxies is a result of both an increase of 15-μm emission and an apparent depletion of 6.7-μm emission. Near-IR together with the mid-IR data make it possible to estimate the relative amount of interstellar matter in the galaxies.

Key words: surveys – galaxies: evolution – galaxies: starburst – infrared: galaxies – infrared: stars.

1 INTRODUCTION

There has been determined effort over the past several years to understand the history of luminous matter in the Universe. Ultimately, one wishes to have a consistent understanding that would tie together the detailed physical processes at work in stars and interstellar medium (ISM) in the Milky Way and local galaxies with the integrated properties of more distant systems. The spectral properties and energy budget of the distant galaxies in turn are crucial in understanding the universal history of star formation, the very faintest source counts and the extragalactic background radiation.

In particular, the infrared (IR) and submillimetre regimes have become the focal point of interest in studies of galaxies, both normal and extreme objects. The near-infrared (near-IR) is an important region for galaxy evolution studies for several reasons. Dust extinction is significantly less hampering here than in the optical, and the light mostly comes from a relatively stable old population of

★E-mail: pvaisane@eso.org

late-type stars, making galaxy colours, counts and *k*-corrections easier to predict and interpret. It is also in the near-IR that the energy output of a galaxy starts to shift from normal starlight to emission re-radiated by the ISM. By 5 μm, the dust emission has taken over from radiation from stellar photospheres, except in most ellipticals.

Apart from the $[12/25] \equiv f_\nu(12\ \mu\mathrm{m})/f_\nu(25\ \mu\mathrm{m})$ colours of *IRAS* galaxies, the mid-infrared (mid-IR) truly opened up for study only with the *ISO* mission (see reviews by Genzel & Cesarsky 2000; Helou 1999). Many studies (e.g. Mattila, Lehtinen & Lemke 1999; Helou et al. 2000) have confirmed the complex nature of the spectral energy distributions (SEDs) of disc galaxies in the 3–20 μm range. In addition to a continuum due to hot (or warm) dust, there are bright IR bands at 3.3, 6.2, 7.7, 8.6, 11.3 and 12.7 μm – these are often called the unidentified infrared bands (UIBs), because of the lack of understanding of their carriers. These broad-band aromatic features are proposed to be the signature of polycyclic aromatic hydrocarbons (PAHs; Léger & Puget 1984).

The PAHs are an essential component in forming the mid-IR [6.7/15] colour ratio, which is emerging as a tracer of star-forming activity in galaxies (Sauvage et al. 1996; Vigroux et al. 1996, 1999; Dale et al. 2000; Helou 2000; Roussel et al. 2001a). The value $[6.7/15] \approx 1$ is expected in quiescent medium and photodissociation regions (PDRs), while H II regions have $[6.7/15] < 0.5$ (e.g. Cesarsky et al. 1996). The [6.7/15] ratio thus remains close to unity for quiescent and mildly star-forming galaxies, while it starts to drop for those with more vigorous star formation activity. This mid-IR flux ratio has also been shown to correlate with the *IRAS* [60/100] colour ratio, which is a well-known indicator of activity level in galaxies (Vigroux et al. 1999; Helou 2000; Dale et al. 2000). A two-component model of a galaxy as a linear combination of differing amounts of cold dust in cirrus clouds and warmer dust in H II regions has been seen as the explanation for the *IRAS* and *IRAS*/*ISO* colour–colour diagrams (Helou 1986; Dale et al. 1999, 2000). On the other hand, the situation might be more complicated (see e.g. Sauvage & Thuan 1994), and for example it is possible that the proportion of star formation in the disc relative to the central region of a galaxy plays a dominant role (e.g. Vigroux et al. 1999; Roussel et al. 2001b).

On another front, deep *ISO* galaxy counts (e.g. Oliver et al. 1997; Taniguchi et al. 1997; Elbaz et al. 1999a; Aussel et al. 1999; Flores et al. 1999 , for ISOCAM counts) have produced surprising results. The differential 15-μm counts show a remarkable upturn below flux densities of 3 mJy and then a rapid convergence at approximately 0.4 mJy. This peak clearly requires strong (luminosity) evolution and can be a result of strong mid-IR emission features, a new population of sources, or some combination of these (Xu 2000; Elbaz et al. 1999b; Genzel & Cesarsky 2000). To understand these results and to develop a coherent picture of early galaxy evolution, it is imperative to learn as much as possible about the more local galaxies.

The ELAIS project (Rowan-Robinson et al. 1999; Oliver et al. 2000) stands as a bridge between the very deep galaxy surveys in the IR, mentioned above, and nearby galaxy surveys (e.g. Boselli et al. 1998; Dale et al. 2000; Roussel et al. 2001a). ELAIS was the largest open time *ISO* project, with the driving ambitious goal to study the unobscured star formation out to redshifts of $z \sim 1$. Source counts in the mid-IR have been published in Serjeant et al. (2000) and the far-infrared (far-IR) counts in Efstathiou et al. (2000).

The aims of this paper are as follows: In Section 2 we present a subset of the ELAIS ISOCAM survey with near-IR follow-up observations. A central new result of this paper, the calibration of the ELAIS data, is performed in Section 2.6 and in Appendix A using the stars detected in our fields. In Section 3 various near- to mid-IR colour–colour diagrams of the ELAIS galaxies are constructed and compared to evolutionary models, including the UIB features in the mid-IR, and to a local *ISO* galaxy sample. In Section 4.1 we attempt to classify sources based on their near- to mid-IR colours. Classifications such as this are expected to be helpful in the future, e.g. with *SIRTF* and *ASTRO-F* data, when large numbers of galaxies with near- and mid-IR fluxes become available without high-resolution spectra accompanying them at least in the first instance. In Section 4.2 we discuss star formation properties of the ELAIS galaxies, and the mid-IR and near- to mid-IR colours as tracers of star formation. Finally, active galaxies and extreme objects are discussed in Section 4.3.

2 OBSERVATIONS AND DATA

2.1 *ISO* data

The mid-IR ELAIS *ISO* observations were made with the ISOCAM LW2 (6.7 μm) and LW3 (15 μm) filters, covering ranges 5–8.5 μm and 12–18 μm, respectively. For a description of the observations, data reduction and source extraction, we refer the reader to Oliver et al. (2000) and Serjeant et al. (2000). At present the final reduction products are available only for the ELAIS southern fields (Lari et al. 2001), and thus we use here the preliminary analysis v.1.3 ELAIS ISOCAM catalogue source list. This is somewhat deeper than the publicly available v.1.4 catalogue[1] but otherwise equivalent (the latter is a subset of v.1.3). At this stage the detections are classified as 'secure' (REL = 2) or 'likely' (REL = 3). However, to have a reliable source list, *we will consider only those detections with near-IR matches*, as discussed below. The reliability and completeness in general of these versions of ELAIS catalogues will be discussed in more detail in Babbedge & Rowan-Robinson (in preparation). Part of our near-IR survey is in the ELAIS N1 region, which was not observed at 6.7 μm.

2.2 Near-infrared data

The near-IR observations were carried out using the STELIRCam instrument at the 1.2-m telescope of the F. L. Whipple Observatory on Mount Hopkins. A description of these *J*- and *K*-band data (taken during 21 nights between 1997 April and 1999 May), reduction as well as photometry can be found in Väisänen et al. (2000). The survey area is approximately 1 deg^2, two-thirds of which is in the ELAIS N2 region (centred at RA $16^{\mathrm{h}}36^{\mathrm{m}}00^{\mathrm{s}}$, Dec. $41^\circ06'00''$) and the rest in N1 (RA $16^{\mathrm{h}}09^{\mathrm{m}}00^{\mathrm{s}}$, Dec. $54^\circ40'00''$). There is a small offset between the simultaneously observed fields of view (FOVs) in the *J* and *K* bands, resulting in slightly different source catalogues in the respective bands.

The 2MASS second incremental data release (Cutri et al. 2000) partially covers the N1 and N2 regions. This allows us to cross-check our bright ($K < 14.5$) photometry directly with 2MASS. This is important also because we will later use 2MASS data in connection with a comparison sample of nearby galaxies from the literature. The 'default' photometry of 2MASS was found to agree very well with our photometry for both stars and galaxies. Our data from Mount Hopkins (while deeper as a result of the longer integration time) are, in fact, taken with a very similar telescope and instrument to the 2MASS data.

[1] Available at http://athena.ph.ic.ac.uk/elais/data.html

Table 1. ISOCAM sources in the 1 deg^2 near-IR survey area within the ELAIS N1 and N2 fields, per band and reliability parameter; REL = 2 stands for a 'secure' detection and REL = 3 for a 'probable' detection. The columns give the total number of *ISO* sources, number of near-IR identifications, and the classification of these matches (see Section 2.5 for the classification). Total numbers for each band are also shown. The row labelled LW2 & LW3 in N2 shows the numbers of sources with a detection in both ISOCAM bands. These objects were already included in the respective LW2 and LW3 rows; the breakdown by the REL parameter is not shown (however, for the galaxies, these can be seen in Table 2).

		Detections	Identified	Stars	Galaxies
N1					
LW3	REL = 2	47	37	7	30
	REL = 3	59	12	1	11
N2					
LW2	REL = 2	170	170	141	29
	REL = 3	53	47	34	13
LW3	REL = 2	68	60	19	41
	REL = 3	115	49	6	43
LW2 & LW3	REL = 2 & 3	53	53	24	29
Totals					
LW2		223	217	175	42
LW3		289	158	33	125

2.3 Matching of mid- and near-infrared data

The ELAIS ISOCAM catalogue has 1322 and 2203 sources in total for *all* ELAIS regions in the 6.7 and 15 μm bands, respectively. These were matched with our near-IR catalogue, which comes from a much smaller area. The ELAIS v.1.3 catalogue includes many double, or even multiple, detections from the edges of neighbouring individual rasters and repeated observations – thus we had to purge the catalogue. We searched for ISOCAM objects separated initially by 1 arcsec, then 3 arcsec and finally 6 arcsec – at each step neighbours were merged if they had the same near-IR counterpart. Ultimately, the matched and purged catalogue consists of 217 and 158 near-IR sources matched with the LW2 and LW3 ELAIS catalogue, respectively. Of these, 53 are common to both ISOCAM filters, and because of LW2 coverage they are all in the N2 region. Table 1 gives the total number of *ISO* sources, the near-IR identifications and their classification per field, filter and reliability class. Notably, *all* those ISOCAM sources detected in both filters were identified, as well as all LW2 sources with REL = 2.

The probability of a chance appearance of, for example, a $K = 17$ mag object within the 6 arcsec search radius is 0.03, estimated from surface densities of near-IR objects (e.g. Väisänen et al. 2000). More than 90 per cent of the matches are brighter than $K = 16.5$ mag – we thus conclude that the purely positional matching is highly accurate. Since we will be using only those mid-IR sources with a near-IR counterpart, we consider the source list to be very reliable.

The ELAIS fields were surveyed also with ISOPHOT at 90 and 175 μm. Since the mid- to far-IR colours of ELAIS sources are discussed in another work (Morel et al., in preparation), we do not discuss them further here, except to note that eight of our 29 galaxies with data from both ISOCAM bands and near-IR photometry also have 90 μm fluxes available. In addition, 20 of the 29 are included in the ELAIS VLA catalogue (Ciliegi et al. 1999).

2.4 Photometry

Since in this work we need to compare fluxes between nearby and distant galaxies, total fluxes are required for both the near- and mid-IR. In Väisänen et al. (2000) we found the 'BEST' magnitudes from SExtractor (Bertin & Arnouts 1996) to be the most robust and accurate over a wide range of magnitudes and source profiles. The Kron-type 'BEST' magnitudes are presented in Table 2, but we calculated also various aperture magnitudes and there is no difference in any final results if large enough apertures are used.

The *ISO* fluxes are measured from characteristic temporal signatures of individual pixels, as described in Serjeant et al. (2000). Instead of conventional aperture photometry, the value of the peak pixel is corrected to total flux using point spread function (PSF) modelling. The adopted correction factors were 1.54 at 6.7 μm and 2.36 at 15 μm. The correction for the LW2 filter is more uncertain because of the much undersampled PSF. Strictly, this correction is appropriate for point sources only, which results in a potentially serious underestimation of fluxes for extended objects. However, the size of the ISOCAM pixel is 6 arcsec, and the large majority of our sources are smaller than this, and we trust that the point source aperture correction gives an accurate value for them. Nevertheless, we examined the largest ELAIS galaxies individually (using their near-IR half-light radii and testing with different apertures) to get an estimate of correction factors to the mid-IR fluxes. We conclude that only four of the galaxies, all of which are included in Fig. 1, definitely need a significant aperture correction. For the largest galaxy in our sample (ELAISC15 J163508+405933), referred to as 'B' in Table 2 and Fig. 1, we adopt fluxes from Morel et al. (in preparation), modified in accordance with our new calibration (Section 2.6). The correction is very large, approximately a factor of 4. The other three galaxies labelled 'A', 'C' and 'D', respectively, are significantly smaller, and for these we adopt an approximate correction factor of 1.5.

2.5 Star/galaxy classification

We plot the near- to mid-IR ELAIS data in Figs 2 and 3 as a function of K magnitude, using all the matched near-IR and ISOCAM detections. We also matched all the sources in our field with optical data from POSS plates using the Automated Plate Scanner data base (APS; Pennington et al. 1993), which includes morphological star/galaxy separation. Those objects with a stellar classification are identified as crosses in the two plots.

Stars clearly seem to lie in regions $[2.2/6.7] > 2$ and $[2.2/15] > 10$. We checked individually all objects in these regions using our near-IR data and were able to correct several ambiguous and erroneous APS classifications (typically optically faint, red objects). There are more stars in the 6.7 μm matches, as expected, and there is more overlap between separate populations in the [2.2/6.7] plot. We verified that several galaxies, likely to be nearby ellipticals, lie in this overlap region, which is shown in more detail in the inset of Fig. 2. Henceforth, those objects which were morphologically verified as stellar by near-IR and/or optical data, *and* have either $[2.2/6.7] > 2$ or $[2.2/15] > 10$, are defined as stars. The rest are then classified as galaxies.

Several sources in the galaxies sample have a stellar APS classification. While we did not attempt a comprehensive morphological classification of the faintest near-IR sources, many of them are obviously extended objects in the near-IR data, and the erroneous APS classification is just due to the faintness of objects. Some of them are, however, point-like also in our data, and thus are potentially interesting cases, to which we will return in Section 4.3. However, this group might still include rare dust-shell stars.

It is interesting to note the proportions of stars and galaxies (see Table 1): in the near- and mid-IR matched catalogue 81 per cent

Table 2. The near-IR sample of ELAIS galaxies detected with both ISOCAM filters. The galaxies are ordered with decreasing 15-μm flux. Columns 7 and 9 labelled 'R' refer to the REL parameter. The coordinates (J2000) are from the near-IR data. The bright galaxies A to E from Fig. 1 are indicated; 'fir' and 'vla' indicate that the object has been detected in the 90-μm ELAIS survey (Efstathiou et al. 2000) and a VLA follow-up survey (Ciliegi et al. 1999); 'q1' and 'q2' indicate a confirmed and potential quasar, respectively, as discussed in Section 4.3.

	RA	Dec.	J (mag)	J error	K (mag)	K error	S_{15} (mJy)	R	$S_{6.7}$ (mJy)	R	Notes
1	16 37 34.4	+40 52 08	13.22	0.02	12.20	0.02	34.3	2	37.3	2	'C', vla
2	16 35 07.9	+40 59 29	12.65	0.01	11.29	0.01	23.0	2	22.2	2	'B', fir, vla
3	16 34 01.8	+41 20 52	13.06	0.01	12.03	0.02	18.5	2	11.8	2	'E', fir, vla
4	16 37 29.3	+40 52 49	12.66	0.01	11.56	0.01	12.9	2	18.9	2	'D', fir, vla
5	16 35 25.2	+40 55 43	14.14	0.03	12.99	0.03	8.8	2	9.0	2	fir, vla
6	16 37 05.1	+41 31 55	15.26	0.04	14.02	0.04	8.5	2	3.8	2	fir, vla
7	16 33 59.1	+40 53 04	14.80	0.04	13.57	0.04	7.6	2	5.3	2	vla
8	16 36 08.1	+41 05 08	15.51	0.03	13.85	0.04	7.6	2	2.7	2	vla
9	16 35 06.1	+41 10 38	15.48	0.04	14.10	0.03	6.2	2	4.9	2	fir, vla
10	16 35 46.9	+40 39 01	15.35	0.04	14.18	0.05	5.6	2	3.0	2	vla
11	16 36 45.0	+41 51 32	14.23	0.04	13.15	0.05	4.9	2	1.7	2	
12	16 36 13.6	+40 42 30	13.44	0.02	12.42	0.02	4.5	2	3.1	2	vla
13	16 36 07.6	+40 55 48	15.83	0.05	14.30	0.05	4.1	2	1.3	2	fir, vla
14	16 37 08.1	+41 28 56	15.26	0.04	13.91	0.04	3.6	2	2.1	3	vla
15	16 37 31.4	+40 51 56	15.47	0.04	14.13	0.06	3.3	2	1.7	2	fir, vla
16	16 34 14.2	+41 03 19	14.79	0.03	13.98	0.04	2.9	2	1.5	3	vla
17	16 34 12.0	+40 56 53	17.59	0.11	15.43	0.08	2.9	2	1.4	2	vla
18	16 37 20.5	+41 11 21	12.92	0.01	11.67	0.01	2.9	2	2.7	2	'A'
19	16 36 09.7	+41 00 18	15.89	0.05	14.45	0.07	2.9	2	1.5	2	vla
20	16 35 19.2	+40 55 57	16.27	0.07	14.90	0.07	2.7	3	0.9	3	vla
21	16 38 51.9	+41 10 53	15.80	0.08	14.27	0.07	2.7	2	2.1	3	
22	16 34 23.9	+40 54 10	15.94	0.06	14.27	0.07	2.6	2	1.6	2	vla
23	16 37 16.8	+40 48 26	14.99	0.03	13.97	0.04	2.6	2	2.1	2	vla
24	16 35 34.0	+40 40 25	18.02	0.15	16.06	0.15	2.3	2	2.1	2	q2
25	16 34 49.6	+41 20 50	15.62	0.04	–	–	2.2	2	1.6	2	
26	16 35 31.2	+41 00 28	17.87	0.17	16.34	0.17	2.2	3	0.8	3	q1
27	16 36 40.0	+40 55 38	16.30	0.06	14.96	0.06	1.9	2	1.3	2	
28	16 34 43.0	+41 09 49	15.60	0.05	14.30	0.06	1.9	3	1.7	2	
29	16 36 15.2	+41 19 12	16.52	0.08	15.07	0.07	1.7	3	0.9	3	

of the 6.7-μm sources are stars; at 15 μm only 21 per cent of the objects are stars.

2.6 Flux calibration of ELAIS ISOCAM data using stars

Before removing the stars from further consideration in this paper, we use them for an accurate flux calibration of the ELAIS *ISO* data. We match observed near- and mid-IR colours to corresponding model colours of IR standard stars, and are able to derive the flux calibration for the ELAIS ISOCAM data with better accuracy than done previously. The derivation is performed in Appendix A: we adopt values of 1.23 and 1.05 ADU gain^{-1} s^{-1} mJy^{-1} for the LW2 and LW3 filters, respectively, i.e. the catalogue v.1.3 values for LW2 and LW3 have to be multiplied by these factors to have fluxes in millijansky. Note that the factors were not included in Figs 2 and 3. [The LW3 calibration is in disagreement with the one performed in Serjeant et al. (2000), where a value of 1.75 ADU gain^{-1} s^{-1} mJy^{-1} was found.] Our values are in good agreement with the ISOCAM handbook values of 2.32 and 1.96 ADU gain^{-1} s^{-1} mJy^{-1} (Blommaert 1998), where an additional factor of 2 correction for signal stabilization has been included (see Appendix A for details). This lends strong support for the accuracy of the reduction and photometric techniques used in the creation of the ELAIS preliminary catalogue.

Furthermore, we can use the bright stars to estimate the completeness of the ELAIS ISOCAM catalogue. Using the mean mid-IR/near-IR flux ratio for stars (see Appendix A and also Figs 2 and 3), we calculate the expected mid-IR fluxes of all bright near-IR stars in our field, and then check whether they actually are included in the ELAIS catalogue. The results are as follows: The 15-μm catalogue is essentially complete above 2 mJy. Below this the completeness begins to drop rapidly. Six stars out of 20 between 1.0 and 2.0 mJy are detected. The 6.7-μm band is essentially complete above 1.5 mJy. The completeness above 1 mJy is 80 per cent, while only 18 out of 73 stars between 0.5 and 1.0 mJy are detected. These numbers are consistent with those derived by Serjeant et al. (2000), who find the 50 per cent completeness limits for the whole ELAIS survey to be ∼1 mJy for both bands (using the calibration of this paper for the 15-μm data).

3 COLOUR–COLOUR DISTRIBUTIONS

3.1 Models

The detailed modelling of near-IR/mid-IR colour–colour distributions and resulting interpretations of physical properties and star formation rates of the galaxies will have to wait for more comprehensive spectral and redshift data. However, it is very informative to check the expected redshift effects on the colour–colour

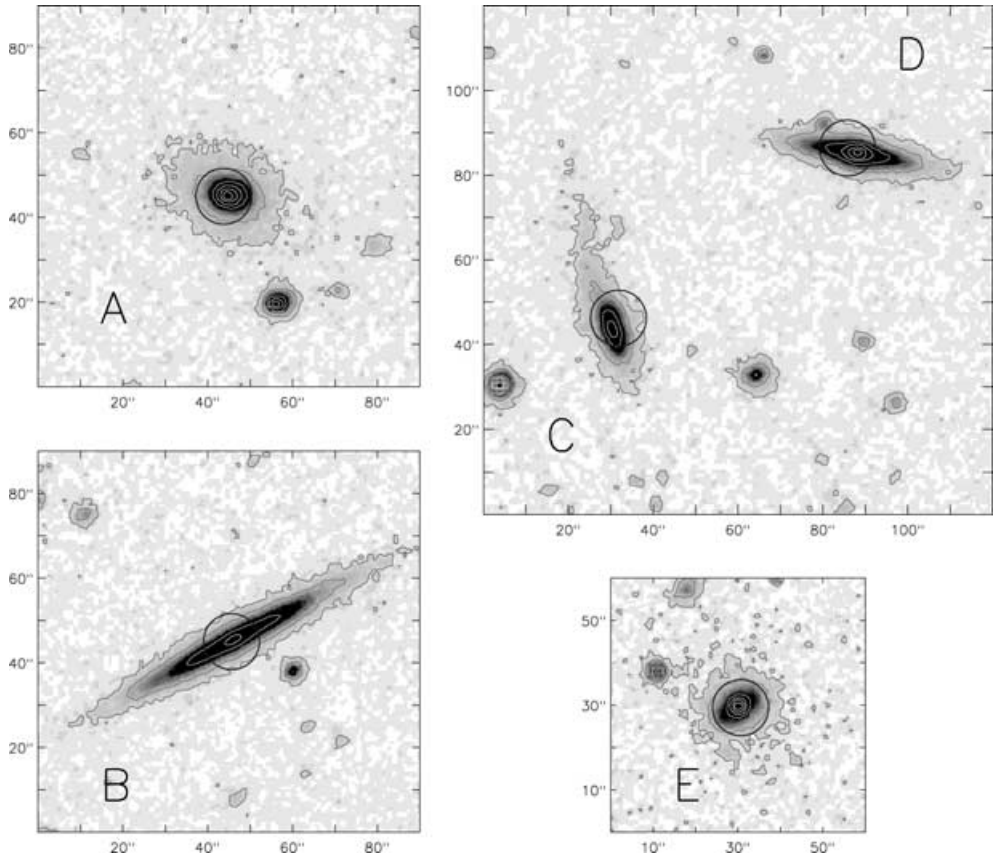

Figure 1. Examples of *K*-band images of the brightest and largest (in near-IR) galaxies in our sample. Positional error circles of 13 arcsec diameter have been plotted around the ISOCAM detections. The ISOCAM pixel size is 6 arcsec. Object 'A' is an E/S0-type galaxy; the NED data base catalogues it with a name NPM1G +41.0441 and unknown redshift. Object 'B' has the largest extent of our sample. It is named UGC 10459, lying at $z = 0.03$ (NED), and it is also a radio source ELAISR20 J163507+405928 (Ciliegi et al. 1999). Objects 'C' and 'D' form a galaxy pair, and 'C' is the brightest mid-IR source in our sample. The pair's redshifts or classifications are not available from the literature. Object 'E' is known as KUG 1632+414 ($z = 0.03$) and it is also a radio and *IRAS* source. NED classifies it as 'spiral' and our near-IR image clearly shows a disc in addition to a very bright unresolved nucleus. The rest of the sources in our catalogue are much smaller.

diagrams. We chose to use a set of models from the GRASIL code[2] (Silva et al. 1998). We used four evolving GRASIL SEDs (elliptical, Sa, Sb and Sc) to compute *k*- and evolutionary corrections and observed colours as functions of redshift, for our *J* and *K* bands as well as the ISOCAM filters. Appropriate filter curves were used to convolve the SEDs, and a colour correction was performed in the case of ISOCAM to be consistent with the convention of measurements (see Blommaert 1998). These four models are used in the following to compare with the data. In addition, to represent a starburst, we simply took the SED of an early-type spiral at the age of 2 Gyr, and held it constant at all epochs. In the wavelength range considered here the SED is similar to that of M82 and also not too unlike Sc in general (see Schmitt et al. 1997; Silva et al. 1998). The cosmology used in the plots is $q_0 = 0.15$ and $H_0 = 50$ km s^{-1} Mpc^{-1}, though changing this does not have significant effects in the redshift ranges considered. It should also be kept in mind that the models represent total luminosity of a galaxy, while the observations in practice are performed with a given aperture (although 'total flux' in photometry is attempted, as discussed above).

[2] Libraries of selected models are publicly available at http://grana.pd.astro.it/grasil/modlib/modlib.html

3.2 Near-IR/mid-IR colours of ELAIS galaxies

In general, the emission from galaxies in near-IR bands is due to the stellar contribution, the 6.7 μm carries information on the PAH contribution, and any strong 15 μm emission would indicate warm dust. There are thus several colour indices that may be useful in studying the relative strengths of these components and processes. For example, the 6.7/15 μm flux ratio is expected to trace activity in the ISM of galaxies.

Figs 4 and 5 show the [6.7/15] ratio against [2.2/15] and [6.7/15]. The first compares the relative strength of the stellar and warm ISM component. Objects to the right are dominated by stellar emission, and those to the left by warm dust, while the vertical axis tells about the heating activity and the relations of PAHs and warm dust. The second figure depicts the stellar versus PAH contribution. To study the [6.7/15] ratio further, the ISOCAM bands are plotted against each other in Fig. 6, normalizing with the near-IR flux, which in addition to stellar light is expected to be a good measure of stellar mass in a galaxy (e.g. Kauffmann & Charlot 1998). The implications of this will be discussed more in Section 4.

Models presented in Section 3.1 are overplotted in all the colour–colour diagrams for the range $z = 0$ to 1. Note that the UIB features move rapidly beyond the 6.7-μm filter with redshift, which results in decreasing [6.7/15] in models including strong PAH emission

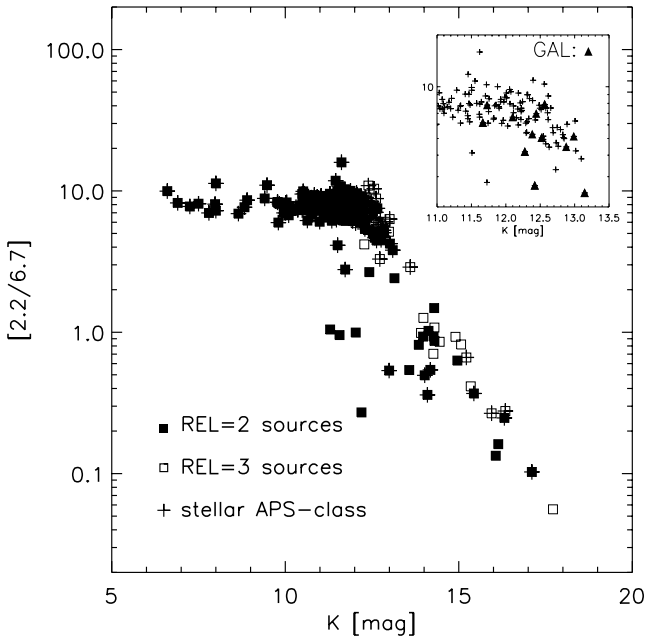

Figure 2. Near- to mid-IR colour as a function of K magnitude ([2.2/6.7] $\equiv f_\nu(2.2\ \mu\mathrm{m})/f_\nu(6.7\ \mu\mathrm{m})$. Those objects which are classified (morphologically) as stellar in the APS catalogue are overplotted with a cross. All the brightest objects are stars. The inset shows a detail of the region where the stellar population overlaps with galaxies (likely ellipticals). Galaxies are plotted as triangles and stars as crosses.

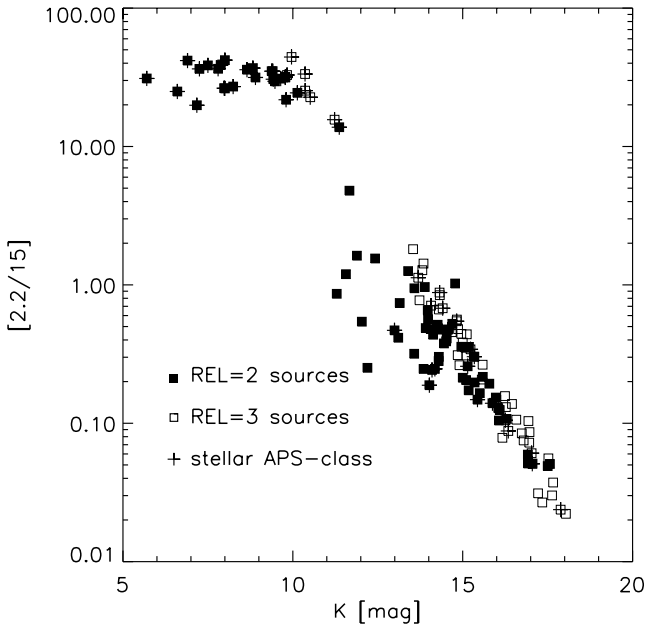

Figure 3. Same as Fig. 2, but showing the K to 15 μm colour.

(especially Sc and starbursts). The colour of Sa-type galaxies, on the other hand, starts to change only at $z \sim 0.75$. Ellipticals at zero redshift occupy the same region as red stars, as expected.

Most of the ELAIS galaxies with data in both mid-IR bands appear to group at a region where the models predict low-redshift, $z = 0.1$–0.4, late-type Sc spirals. According to the models, the near- to mid-IR SEDs of all spirals would look fairly similar at $z \sim 1$. However, it is unlikely that such objects are detected to the ELAIS survey limits.

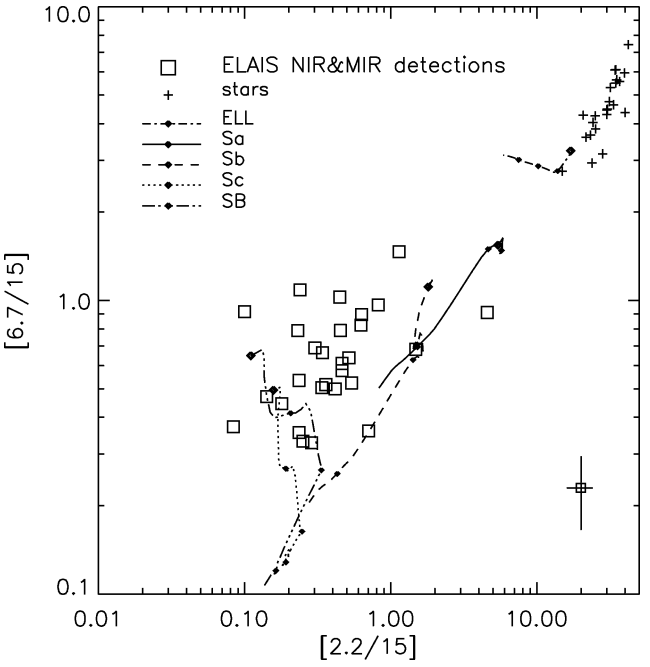

Figure 4. The [6.7/15] mid-IR colour ratio versus [2.2/15] colour of all ELAIS sources in our fields. Those objects which were previously defined as stars are shown as crosses. GRASIL model predictions for galaxies are overplotted. The model colours are for a range of $0 < z < 1.0$, with the largest solid symbol marking $z = 0$ and the others the positions for $z = 0.25$, 0.5 and 0.75. Average, conservative error bars are shown at the lower right corner.

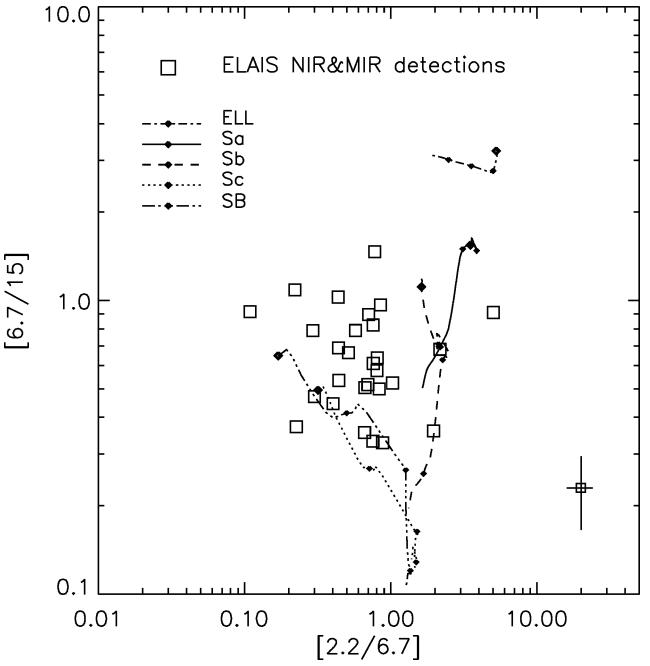

Figure 5. The [6.7/15] ratio versus [2.2/6.7]. Typical error is again indicated at lower right corner.

Active galactic nuclei (AGN) on the other hand are expected to lie at the extreme upper right in Fig. 6 owing to their steeply rising continuum (e.g. Laurent et al. 2000).

The two mid-IR filters detect surprisingly different populations. As can be seen from Table 1, of the 97 identified galaxies that are

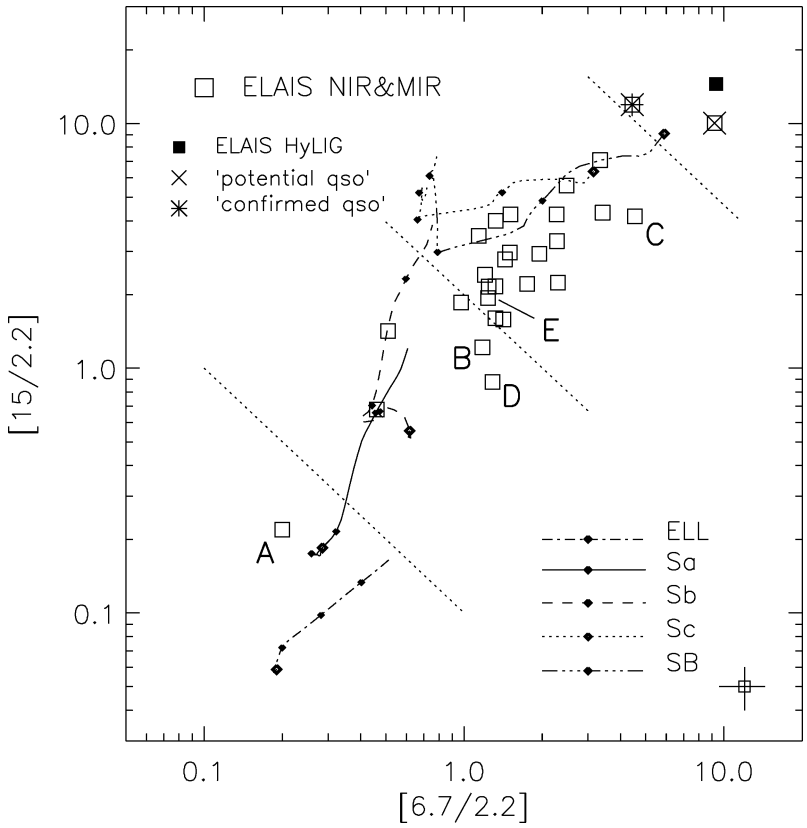

Figure 6. The 6.7 and 15 μm fluxes normalized with the *K*-band flux, i.e. by the stellar contribution to the brightness of the galaxy. The strengths of the mid-IR fluxes are seen to correlate strongly, and the difference in the relative strength of mid-IR flux ranges over nearly two orders of magnitude. The GRASIL models are overplotted again. The bright galaxies of Fig. 1 are labelled from A to E. The dotted lines roughly separate areas for different types of galaxies – see Section 4.1. In addition, we have overplotted a hyperluminous IR galaxy ($z = 1.1$) detected in another ELAIS field (see Morel et al. (2001)) and two 'potential quasars' discussed in Section 4.3, one of which is a confirmed QSO at $z = 1.14$. Typical error is shown at bottom right corner.

from an area covered with both mid-IR bands, only 29 are common to both LW2 and LW3. There are 55 galaxies detected only at 15 μm, and 13 galaxies detected only at 6.7 μm. For those ISOCAM sources with a detection in only one mid-IR band, the $J - K$ colour might provide additional clues. For example, starbursting galaxies should have very red $J - K$ colours. Fig. 4 plots the [2.2/15] against $J - K$. While there are a number of sources with a red $J - K$, they do not constitute a large population. More strikingly, compared to Figs 4 and 6, there are many more sources at a low [2.2/15] ratio.

While the most extreme sources are too faint to acquire any definite morphological information from our data, we can constrain the nature of the sources missed in the 6.7-μm band by examining detection limits. Since the 15-μm fluxes of the missed 51 galaxies range from 1 to 3 mJy, typical [6.7/15] ratios should be around 0.45 to be consistent with the 80 per cent LW2 completeness detection limit. This implies Sc galaxies or starbursts around $z \approx 0.15$ or Sb at $z \sim 0.5$. Accordingly, most [2.2/15] ratios of the missed sources (empty squares in Fig. 7) do lie by the Sc and starburst model curves. We also derived a rough estimate for the expected 6.7-μm flux from a mean correlation of [15/2.2] with [6.7/2.2], using the ELAIS sources in Fig. 6 and also a comparison sample discussed below in Section 3.3. The derived f_ν(6.7 μm) are shown in Fig. 8. Galaxies with the lowest [2.2/15] ratios fall below the LW2 detection limit while still being detected in LW3. It is thus clear that the faintest late-type spirals and starbursts make up the majority of LW2-missed sources. However, statistically we should find only approximately five sources with LW2 fluxes between 1 and 2 mJy in the figure. There are around 20, many of them with a [2.2/15] ratio typical of earlier type spirals (Sb). These might harbour some form of activity resulting in a lower than expected [6.7/15] ratio.

The objects seen in 6.7 μm but not in 15 μm are plotted in Fig. 9. As seen there and in Fig. 8, almost half of the LW3-missed objects appear to be ISM-deficient early types. However, since the LW3 catalogue should be more than 90 per cent complete above 2 mJy, the derived f_ν(15 μm) at least for some of the galaxies might be too high. Surprisingly, two confirmed quasars (QSOs) are among the LW3-missed objects (see Section 4.3). However, numbers are small, and the 6.7-μm fluxes are low, close to the detection limit, so it is difficult to conclude anything definite.

3.3 Comparison sample

In order to compare our resulting ELAIS near- to mid-IR colours to a local sample of galaxies observed with *ISO*, and to discuss how well the galaxy types can be separated with near- and mid-IR colours, we made use of the data sets of Boselli et al. (1998), Dale et al. (2000) and Roussel et al. (2001a). Naturally, there exists a large body of work performed with *IRAS* galaxies establishing near- and mid-IR data bases (e.g. Spinoglio et al. 1995) – however, to avoid complications of band conversions, we restrict ourselves only to recent *ISO* data. The Roussel et al. set consists of nearby spirals, and it includes a subset of the Boselli sample, which are Virgo cluster galaxies. The Dale et al. sample contains galaxies from the *ISO* US Key Project 'Normal Galaxies'.

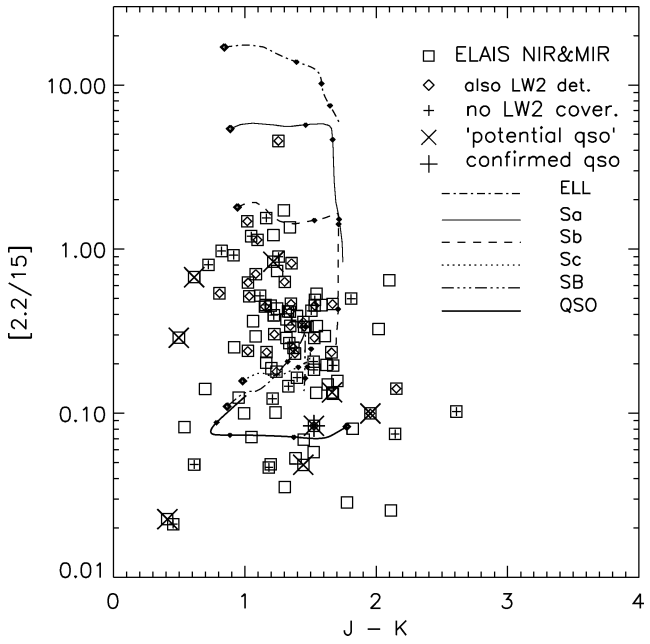

Figure 7. The [2.2/15] ratio plotted as a function of $J-K$ colour. For most normal galaxies $J-K$ is expected to be between 1 and 2. Those sources which are detected in both mid-IR bands are marked with a diamond, and those which do not have LW2 coverage are marked with a cross. Most of the sources missed by the 6.7 μm survey (i.e. empty squares) have a very small [2.2/15] ratio, expected from moderate-redshift Sc and starburst galaxies as predicted by GRASIL. See Fig. 8 for more details. One confirmed QSO ($z=1.142$) is marked with a large asterisk, and 'potential QSOs' discussed in Section 4.3 are marked with large diagonal crosses. The QSO model (from Schmitt et al. (1997)) curve is marked at half-redshift intervals, while other models are with 0.25 intervals, as before.

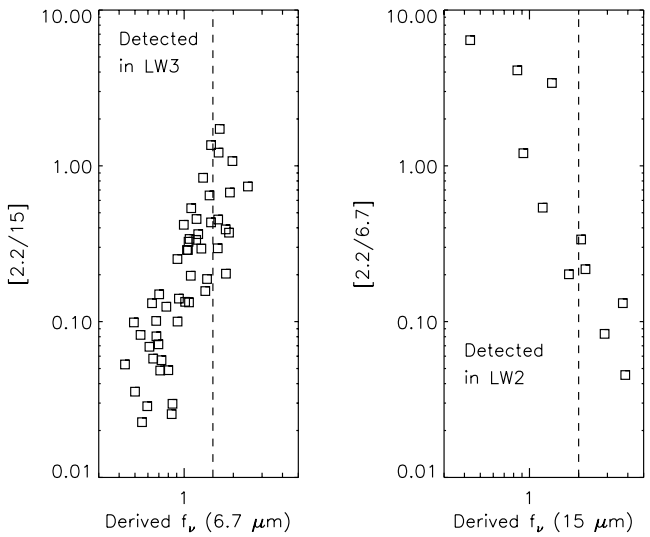

Figure 8. Galaxies detected in only one ISOCAM filter. Fluxes in the other band are derived from their expected correlation to near-IR/mid-IR ratio using models, ELAIS galaxies and local galaxies discussed in Section 3.3. The dashed vertical lines show the expected completeness levels. Those detected at 15 μm but missed in the 6.7 μm band are plotted on the left. According to [2.2/15] these galaxies should typically be Sc, starbursts and perhaps AGN. Galaxies detected in 6.7 μm but missed in the 15 μm band are on the right. Many of the missed galaxies are early types with high [2.2/6.7], though there are also QSOs included.

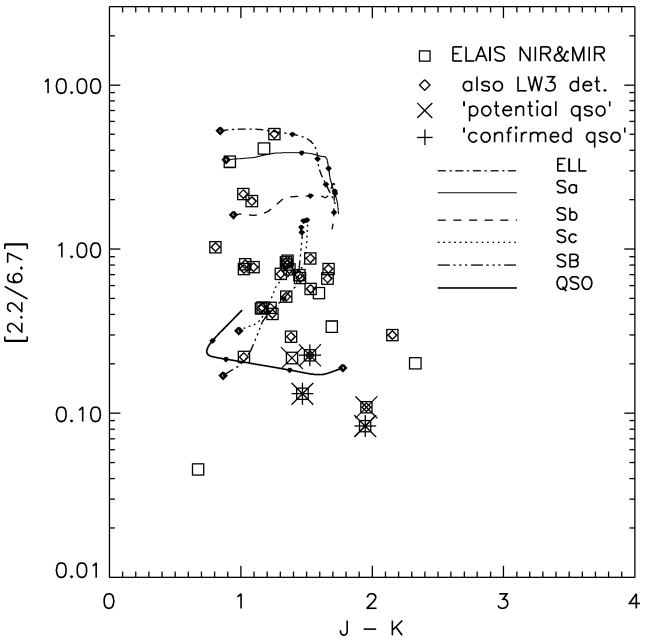

Figure 9. The [2.2/6.7] ratio plotted against $J-K$ colour. Some of the objects missed by LW3 seem to be nearby early-type galaxies. In fact, there are several more such cases, but they lack coverage in one or the other near-IR band. Other LW3-missed objects have low [2.2/6.7] and lie close to the QSO model curve. 'Potential QSOs' discussed later in Section 4.3, are marked with large diagonal crosses; three of these are actually catalogued quasars and are overplotted with a large cross (only one of them is detected by LW3).

The main difficulty in the comparison is the various photometric techniques used in both the near-IR and *ISO* data (see e.g. Spinoglio et al. 1995). A large number of the nearby galaxies have near-IR data available from NED (the NASA/IPAC Extragalactic Database). However, to have consistent photometry, we decided to use only those galaxies for which there were 2MASS data available from the second incremental data release. The 2MASS catalogue lists numerous magnitudes, of which we used the default 'fiducial circular magnitudes at 20 mag/sq. arcsec', because of the wide range of sizes and shapes of the galaxies in the comparison sample.

Boselli et al. (1998) give their own near-IR photometry. We performed a cross-check of their *K*-band photometry between 2MASS values and found a fairly good consistency: apart from some Sc-type galaxies, 2MASS isophotal magnitudes were 0.15 mag fainter than the Boselli values, with a scatter of 0.31 mag. That the levels of Boselli and 2MASS magnitudes are so close, and that the sizes of galaxies in the other two samples are not significantly different from the Boselli galaxies, gives us confidence to use 2MASS magnitudes for the nearby comparison galaxies, and to compare them directly with the 'total magnitudes' of the ELAIS objects. Nevertheless, for consistency reasons with the Dale and Roussel samples, we decided to use only those galaxies from Boselli et al. which had 2MASS photometry available. In the following, with the Dale and Roussel samples we mean those galaxies from the respective original works for which we found 2MASS magnitudes. Our Boselli sample means those galaxies from Boselli et al. with 2MASS photometry, and those galaxies excluded which are already included in the Roussel sample.

As for the *ISO* data, the standard CAM Interactive Analysis (CIA) packages were used for preprocessing of raw data in all of the

comparison data here, as well as the ELAIS data. The *ISO* fluxes of all the comparison samples are calculated from *maps* resulting from the application of CIA/IDL procedures [see Roussel et al. (2001a) for a detailed description of the reduction process]. Fluxes in all these comparison samples were calculated using various apertures, and all claim their fluxes to represent total values at better than 20–30 per cent accuracy. There is a systematic difference by approximately a factor of 1.4 in fluxes of some galaxies common to the Roussel et al. and Dale et al. catalogues (see Roussel et al. 2001a); however, none of these are included in our subsamples. The mid-IR fluxes in Boselli et al. (1998) are not published apart from SED plots; the values were provided by A. Boselli.

As mentioned earlier, in contrast to the photometry of these comparison samples, the mid-IR ELAIS fluxes are values derived from peaks in time histories of individual pixels and corrected for PSF effects. However, we are confident that the ELAIS ISOCAM fluxes are close to the true total values (see Sections 2.4 and 2.6 and Appendix A).

4 DISCUSSION

4.1 Classifying ELAIS galaxies

Unfortunately, at present we do not have optical imaging to definitely classify our ELAIS galaxies. Classification with the help of GRASIL models was briefly discussed along with near-IR/mid-IR colours in Section 3.2. How accurate can the classification of normal galaxies be using near- and mid-IR colours? For example, Sauvage & Thuan (1994) find only loose correlations between *IRAS* colours and morphological type in their large sample. There would be interest in having a near-IR/mid-IR photometric classification, in anticipation of forthcoming very large galaxy surveys by, for example, *SIRTF*. Here we will investigate whether the comparison sample presented above has correlations between morphology and near-IR/mid-IR properties and see what these would imply for our ELAIS galaxies.

Fig. 10 shows the Roussel and Boselli samples in a mid-IR/near-IR two-colour diagram along with ELAIS sources. There is a clear trend: the type of galaxy becomes systematically later upwards along the diagonal. This should not be a great surprise, since essentially the progression shows the overall amount of emission from the ISM in the galaxy increasing. The average [15/2.2] for early types (Sa and earlier) is 0.2 whereas for the late types (Sc and later) [15/2.2] ≈ 2.2.

Fig. 11 shows the Dale sample in the same fashion. The sample covers a wide range of morphological types, but it is evident that barred galaxies are plentiful and especially galaxies that have been attached with a peculiar ('p') morphology in addition to a regular Hubble type. The trend seen in the Roussel and Boselli samples is not clear at all. The whole sample groups strongly towards the Sc model colour, including the morphological early-type galaxies. The peculiars ('p' and purely 'Pec') and irregulars tend to have the highest mid-IR/near-IR ratios.

The Dale sample also has many more galaxies with significantly lower [6.7/15] compared to the Roussel/Boselli sample. The difference mainly comes from galaxies with high mid-IR/near-IR ratios. This is true regardless of the ~40 per cent discrepancy in the photometry mentioned earlier. The Boselli and Roussel galaxies

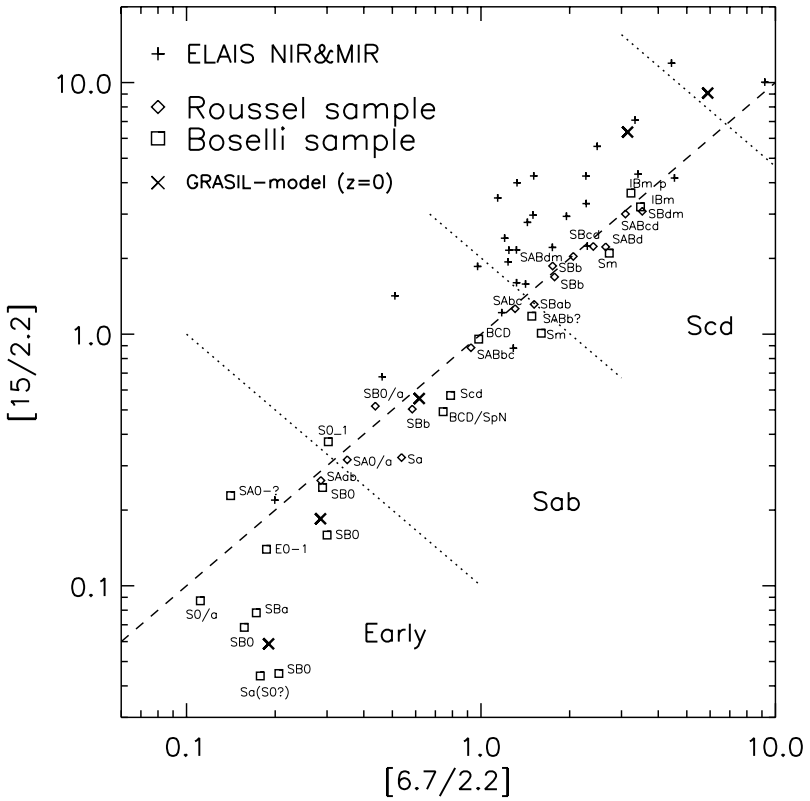

Figure 10. The 6.7 and 15 μm fluxes from Roussel et al. (2001a) and Boselli et al. (1998), normalized with the *K*-band fluxes. Corresponding near-IR data are from 2MASS. The ELAIS data are overplotted as small crosses and the GRASIL models are shown for $z = 0$ only (see Fig. 6 for redshift dependence). The dashed line shows the one-to-one ratio of 15 and 6.7 μm fluxes. We have separated regions roughly corresponding to different types of galaxies with dotted lines – see text for details.

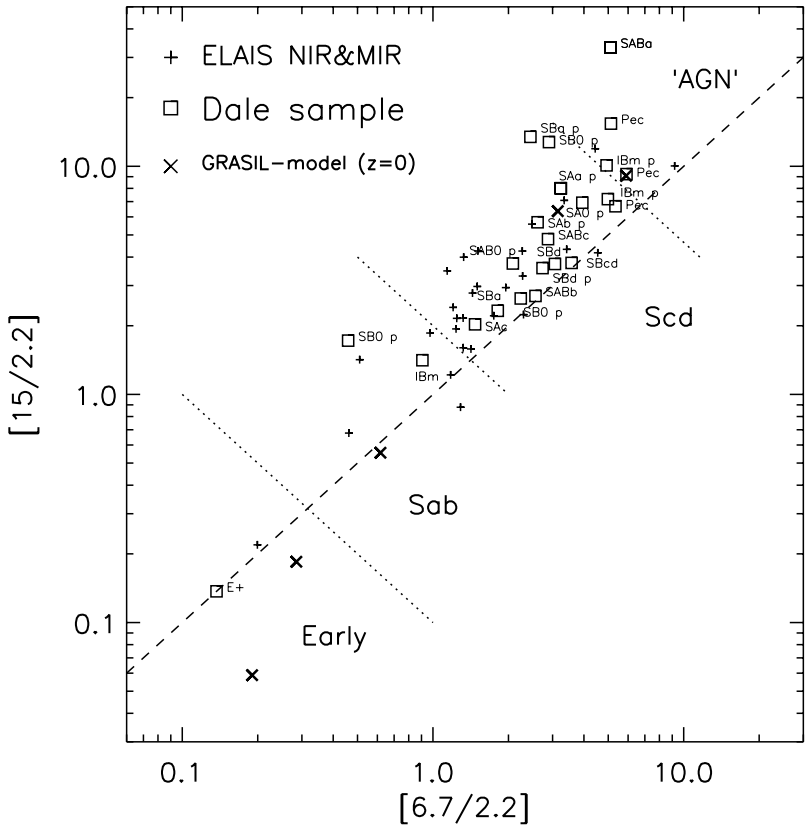

Figure 11. The 6.7 and 15 μm fluxes from Dale et al. (2000) normalized with the *K*-band flux. Near-IR data are from 2MASS, except for the galaxy in the lower left region (NGC 6958, NED magnitude; included merely to have one example of an elliptical). The region loosely labelled 'AGN' is expected to include sources such as QSOs, ULIRGs and strong starbursts. ELAIS data, GRASIL models, and dashed and dotted lines are presented as in the previous figure.

on the other hand are strongly concentrated along the one-to-one correlation line where $[6.7/15] \approx 1$, where the galaxies are supposedly dominated by quiescent ISM. We will return to this point in Section 4.2.2.

As can be seen in Figs 10 and 11, we have divided the diagram into four regions with the dotted lines: the areas roughly correspond to low-redshift early-types, Sab spirals, Scd, and 'AGN' [the latter class includes several types of active sources, e.g. QSOs, Seyfert nuclei, ultraluminous infrared galaxies (ULIRGs), strong starbursts]. The dividing lines in the figures can be obtained from $\log[15/2.2] = -\log[6.7/2.2] + b$ where $b = -1.0$, 0.3 and 1.67 starting from the lower left, respectively. The Roussel and Boselli galaxies fall very well into their areas. Disregarding blue compact dwarfs (BCDs), there are only six galaxies out of 34 in a 'wrong' area, and of these, five are very close to the borderlines. This classification does not work as well for the Dale sample though. We conclude that according to the nearby comparison sample the near-IR/mid-IR two-colour diagrams do discriminate between types of normal galaxies, especially those which have $[6.7/15] \approx 1$.

Where are our ELAIS galaxies in this classification? The ELAIS sample as a whole clearly groups towards the late Hubble types. However, as seen above, near-IR/mid-IR flux ratio may not be a good indication of morphological type for those galaxies with low [6.7/15]. Nevertheless, of the 29 galaxies in Table 2 (see Fig. 6) there are 21 galaxies in the Scd region and five in the Sab region. Two are found in the uppermost region in the far right – in Section 4.3 they are shown to be potential AGN. Only one galaxy seems to be an early type, though it does have excess 15-μm flux. Indeed, early-type galaxies have been shown to have widely differing amounts of dust (see Madden, Vigroux & Sauvage 1999, and references therein). 'Traditional' ellipticals, with no significant ISM presence, would not have been seen at all by the LW3 filter in the ELAIS survey. As shown in the inset of Fig. 2, there are several probable ellipticals that are detected only in LW2.

All the largest galaxies that show clear morphology in our data (Fig. 1, i.e. those labelled in Fig. 6) are in consistent classification areas: 'A' is the early-type galaxy and the rest are spirals. Object E is a disc galaxy with a very bright compact nucleus. It has the lowest [6.7/15] ratio of these five bright galaxies, indicating star formation, as will be discussed next.

4.2 Tracing star formation activity

4.2.1 Star formation tracers

Much-discussed tracers of star formation include the Hα emission of a galaxy, the UV continuum and total far-IR luminosity. It is also well known that star formation in galaxies occurs in two very distinct places: in the discs of spirals, and in compact circumnuclear regions (for a comprehensive review, see Kennicutt 1998). In principle the mid-IR could help in solving some of the uncertainties related to the mentioned diagnostics: e.g. mid-IR is certainly less prone to extinction than UV and Hα studies. It could also help in determining the heating source of IR emission, which affects the accuracy of the far-IR diagnostic. The far-IR tracer is known to work well for circumnuclear starbursts – it is in the discs of normal galaxies where help would be needed.

If the mid-IR is to be useful as a star formation rate (SFR) indicator, calibrators with the other methods are necessary because of the complexity of theoretically deriving an accurate relation between mid-IR emission and amount of young stars. Indeed, Hα emission has been shown to correlate with mid-IR luminosity *in the discs* of spiral galaxies (Vigroux et al. 1999; Cesarsky & Sauvage 1999; Roussel et al. 2001b). Also far-IR seems to correlate linearly with mid-IR and Hα if only discs are considered, and SFR can thus be estimated (Vigroux et al. 1999; Roussel et al. 2001b). The relations do not hold in regions of more intense star formation (e.g. nucleus), and thus nuclear star formation could confuse a global SFR determination. Vigroux et al. and Roussel et al. argue that this is precisely the reason for non-linearity in global far-IR versus Hα relations. Thus, only limits to SFR can be calculated from integrated mid-IR luminosity, and the need for information on the proportions of disc and nuclear IR emission is highlighted.

4.2.2 *Clues from $f_\nu(6.7\mu m)/f_\nu(15\ \mu m)$ and near- to mid-IR*

The mid-IR flux ratio is helpful in tracing the star-forming activity, as discussed before. We also expect the near-IR to add to the information. To illustrate these effects, Fig. 12 shows all those galaxies from the comparison sample discussed in Sections 3.3 and 4.1 which had *IRAS* fluxes available. The upper left panel shows an *IRAS* colour diagram and upper right the *ISO-IRAS* colour distribution. The lower panels plot the near-IR/mid-IR colours against the *IRAS* [60/100] colour. The galaxies are differentiated by morphology into ellipticals/lenticulars, discs and irregulars/peculiars – a galaxy may have both a lenticular or disc and a peculiar classification.

The previously observed trend (Helou 1999, 2000; Vigroux et al. 1999; Dale et al. 2000), that [6.7/15] first remains fairly constant and starts to drop only at a higher [60/100] level, is evident. While there is more scatter between galaxies in the near-IR/mid-IR ratios at low [60/100] values, the [2.2/15] value does (anti) correlate closely with [60/100]. In contrast, the slope of [2.2/6.7] has a break. Empirically, examining the lower panels, it is clear that the drop in [6.7/15] is caused by the stronger increase of 15-μm emission relative to that at 6.7 μm. Also, the [6.7/15] and [2.2/6.7] slopes have almost exactly inverted shapes, which results in the linear [2.2/15] versus [60/100] relation.

What then do the slopes of colour indices tell us? First of all, the nearly constant [6.7/15] at [60/100] < 0.4 heating regime might imply that both mid-IR bands are dominated here by emission from a common source, namely the UIBs, as suggested by Roussel et al. (2001b). On the other hand, since the 11.3 and 12.7 μm UIB bands contributing to the LW3 filter are thought to be weak, it might also be a common *site* of the emission, rather than common physical origin, which is more important. Nevertheless, at higher heating levels the global levels of 6.7 and 15 μm emission clearly behave differently. A simple and common interpretation of the drop in the [6.7/15] ratio has been that, after a threshold, the heated continuum from very small grains enters the 15-μm band. If this were the *only* effect, one should expect also a break in the [2.2/15] slope, which is not seen. Since the strength of PAH emission would be expected to follow the interstellar radiation field (ISRF), the break in [2.2/6.7] could be taken to indicate the depletion of UIBs in galaxies with hottest [60/100] [see Cesarsky et al. (1996) for the effect in localized intense radiation environments]. The *ISO-IRAS* diagram must then be explained by both the increasing 15-μm emission and decreasing (relative to ISRF) 6.7-μm emission.

Are these effects driven mainly by differing amounts of quiescent and active media in the galaxy as a whole (as in the two-component model; Helou 1986; Dale et al. 1999), by different proportions of

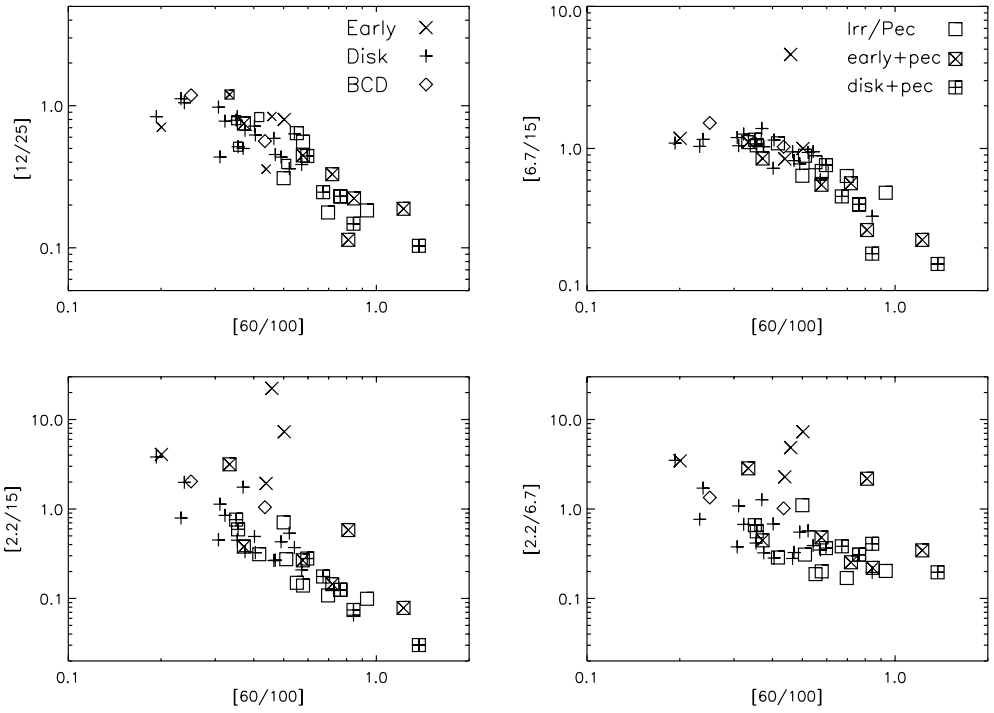

Figure 12. Comparing the *IRAS* [60/100] colour and star formation tracer to near- and mid-IR colours of all the comparison sample galaxies with available *IRAS* fluxes. Early types (until Sa), disc galaxies, irregulars and BCDs are plotted with different symbols. Those classified as peculiar are overplotted with squares. Note that most of the early-type Boselli galaxies had only upper limits in the *IRAS* data, and are not plotted (they would populate the relatively empty region at [6.7/15] > 2 in the upper right panel).

star formation happening in the disc versus the central parts (e.g. Vigroux et al. 1999; Roussel et al. 2001b), or something else? To study this in detail is beyond the scope of the present paper, and in any case cannot be done only with integrated, global values. However, it is interesting to note the trends with the morphologies. The galaxies with constant $[6.7/15] \sim 1$ are mainly normal disc galaxies, and, in fact, their spread in [2.2/15] and [2.2/6.7] is correlated with their Hubble type as already seen in Section 4.1. Those with higher [60/100] span all morphological types, but stand out by having been classified as peculiar one way or another (more active nuclear regions?). Thus, it appears that at lower heating levels ($[60/100] \gtrsim 0.4$) the near-IR/mid-IR (and far-IR) colours of galaxies are driven by morphology, i.e. by the spatial distribution of the ISM. At higher [60/100] the trends on the other hand follow closely the increasing radiation field, the warming dust continuum and (possibly) the destruction of PAH carriers. This is in agreement with the mid-IR/far-IR studies of Sauvage & Thuan (1994), who find the far-IR colours along the Hubble sequence to be driven by both star formation efficiency and spatial distribution of dust.

4.2.3 Nuclear star formation

As seen in Fig. 12, there are several early-type galaxies in the high [60/100] region of the panels. These must have strong nuclear star formation since the mid- and far-IR colours of the galaxies are totally dominated by a starburst. However, it is interesting that the inclusion of near-IR photometry distinguishes several galaxies with high near-IR/mid-IR ratios which otherwise are tightly placed within the main group of points in the *IRAS* and *ISO-IRAS* plots. These are also all early types, but apparently not true starbursts. They simultaneously have relatively high heating levels (especially one at $[60/100] \approx 0.8$, NGC 1266) and high near-IR/mid-IR ratios, typical of more normal lenticulars. This may suggest, for example, that centrally concentrated dust is heated by the high ISRF environment found in the centres of ellipticals and lenticulars (Sauvage & Thuan 1994). However, we also note that all six galaxies at $[2.2/6.7] > 2$ (after excluding one elliptical) have signs of nuclear activity: five are low-ionization nuclear emission regions (LINERs) and one has an Sy2 nucleus. It thus seems that the use of the near-IR/mid-IR ratio picks out galaxies with weak active nuclei from the mid-IR/far-IR sequence. Galaxies that are fully dominated by an AGN are expected to have a much higher [60/100]. For example, the most extreme source at lower right in Fig. 12 is an AGN (NGC 4418; Roche et al. 1986; Spoon et al. 2001).

We also note that the four Dale galaxies with the lowest [6.7/15] ratios are all barred early-type spirals (SB0 to SBa). They have on average $[6.7/15] \approx 0.4$, while the overall average is $\approx$0.6. Two out of five of the strongly barred early-type galaxies have quite normal [6.7/15]. Though the statistics are weak, this fits very well with the findings of Roussel et al. (2001c), from a different galaxy sample, that in some early-type barred galaxies there is excess 15-μm flux due to recent star formation triggered by bar-driven gas inflows. Barred galaxies in general however do not seem to have greater star-forming activity than the non-barred cases.

4.2.4 Star formation in ELAIS galaxies

The ELAIS galaxies have on average $[6.7/15] \approx 0.67 \pm 0.27$, which indicates that the majority of them seem to be star-forming. While some of the sources might be at redshifts that warrant a significant correction to acquire the true ratio, most of the objects are expected to lie at small redshifts, $z < 0.3$. This is strongly suggested by Figs 4 and 5 (see discussion in Section 3.2). The same redshift range can also be derived from typical near- and mid-IR fluxes. The median K magnitude of the galaxies with detections in both mid-IR filters is 14.1 mag, which gives an expected median redshift of $z \approx 0.15$ (Songaila et al. 1994). Flores et al. (1999) obtained spectroscopy for a deeper sample of 15-μm ISOCAM galaxies and found a median redshift of $z \sim 0.7$. Our galaxy sample is an order of magnitude brighter, thus indicating typical redshifts of $z \sim 0.2$ or less. If only identified LW3 ELAIS galaxies are considered, the median redshift could maximally be at $z \sim 0.3$. As seen, for example, from Fig. 4, k-corrections of Sc and starbursts decrease the [6.7/15] ratio by a factor of $\sim$2 out to a redshift of $z \approx 0.4$. The effect is much smaller for earlier types. The redshift-corrected [6.7/15] ratios are thus likely to stay below the quiescent $[6.7/15] \sim 1$ value. The lowest detected [6.7/15] are at $\sim$0.3, which would indicate significant dust heating: $[60/100] \sim 0.6$–0.9, allowing for redshift effects in the 6.7-μm band.

A rough estimate of star formation rates (SFR) expected can be made utilizing relations in Roussel et al. (2001b). They found a good correlation between mid-IR emission and Hα, and thus SFR. The correlation holds only in discs of spirals, however, or globally only in galaxies where the integrated flux is dominated by the disc. From our sample, we selected quiescent and likely disc-dominated sources, i.e. those with [6.7/15] close to unity and falling, which fell into the 'Scd' area in our classification. There are eight such sources, six of which with $K \sim 14$ mag. Assigning these a redshift of $z = 0.17$ and using blindly the SFR relations from Roussel et al. (2001b), with assumptions and filter widths therein, the average SFRs translate to $\sim$15–30 $M_\odot$ yr^{-1}. Some of the fainter ELAIS galaxies would get SFRs several times this value; however, the application of the relation is highly uncertain without more information of the sources. The two remaining objects of the selected eight are those labelled 'C' and 'D', the bright galaxy pair in Fig. 1. These lie at about $z = 0.03$, and would come out with SFR ($M_\odot$ yr^{-1}) $\approx$ 7 and 3, respectively.

Finally, we note that many of the ELAIS sources (as the pair just mentioned) appear to be part of a double or multiple system, some with disturbed morphology. Tidally triggered star formation clearly plays an important role in mid-IR studies of galaxies. We have verified this trend with deeper near-IR follow-up observations of the faintest (and blank field) *ISO* detections using the *IRTF*; the results will be discussed elsewhere.

4.3 Quasars, active galactic nuclei and extremely red objects

As shown, for example, in Laurent et al. (2000), the signature of AGN is a strong rising continuum starting already at 3 μm. Returning to Figs 6, 7 and 9, we further investigated the sources with low near-IR/mid-IR ratios, in order to check the capability of near-IR/mid-IR for AGN/QSO detection.

Making use of the APS colours, Fig. 13 shows the $R - J$ colour (R being the POSS 'E' magnitude) against $J - K$. The solid symbols are the near- and mid-IR ELAIS galaxies, while we have also marked the stars with small symbols. This plot is equivalent to those used in optical/near-IR searches for (obscured) QSOs (the 'KX method'; see Warren, Hewett & Foltz 2000; Francis, Whiting & Webster 2000; Barkhouse & Hall 2001). In general, QSOs tend to have red $J - K$ colours in contrast to a blue $R - J$ (or B or V instead of R).

We first selected from our galaxy sample those objects which had a stellar or ambiguous morphology from APS (20 objects in total; see also Figs 2 and 3). We checked each of these individually from our near-IR data, and many turned out to be galaxies. Several were,

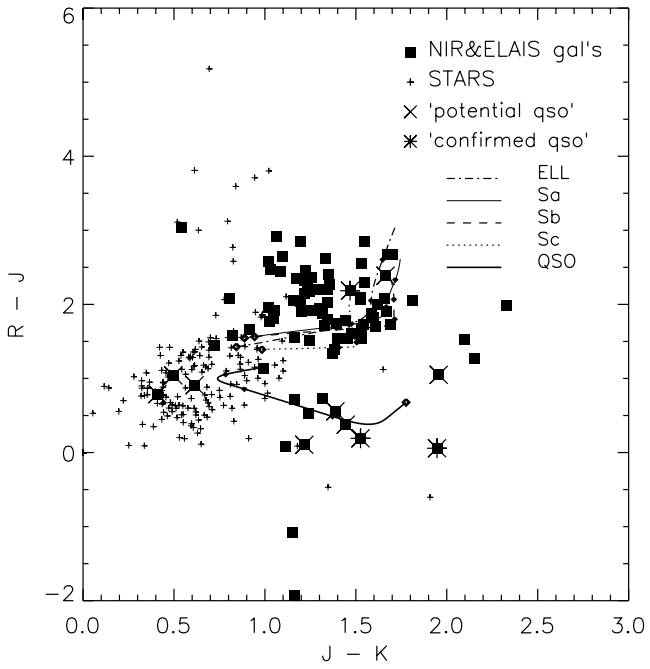

Figure 13. $R-J$ plotted against $J-K$ colour. The solid symbols are the ISOCAM galaxies (one or both filter detections). The ISOCAM detections classified as stars are overplotted as small crosses. Most stars occupy the lower left region, while dwarf stars rise to red $R-J$ colours. Those galaxies, which morphologically seem point-like, or are too faint to be classified morphologically from our near-IR data, are overplotted as large crosses. Three of these turn out to be catalogued quasars, and are marked with an asterisk (shown also in Figs 7 and 9). Models are overplotted as before.

however, either point-like or too faint to classify: these 'potential QSOs' are overplotted with large diagonal crosses in Fig. 13, and also in Figs 7 and 9. It is quite interesting that the majority of these do, indeed, fall by the near-IR/mid-IR colours predicted for QSOs/AGN (note that the selection was done only by optical/near-IR colours and morphology). All the five potentials with 6.7-μm flux have a very steep K to 6.7-μm gradient. Since the selection here required a POSS detection, the faintest near-IR objects are excluded – for example, the three lowest empty squares in Fig. 7 at $J-K>1.3$ are also point-like to our resolution, and have near- and mid-IR characteristics similar to the 'potential QSOs'.

Part of our N2 region is covered by the Crampton et al. (1988) quasar catalogue. Three of the 'potential QSOs' are found in the catalogue (and are marked with a large asterisk in the figures mentioned), which demonstrates the usefulness of the KX method. Note that this does not rule out that other potentials, specifically among those seven with $J-K>1.4$, could not be QSOs due to only a partial overlap with the quasar catalogue. The two points at $R-J>2$ are optically faint, near the APS limits, and are brought down to the 'QSO area' when using near-IR/mid-IR. Three of the potentials have a very blue, star-like, $J-K$; on the other hand they have clear mid-IR excess as evidenced by LW3.

Oddly, only two of these 'potential QSOs' have both ISOCAM filter data available – in Figs 4 and 5 these two are the points with the smallest near-IR/mid-IR ratios. As seen in Fig. 6, they are indeed the two ELAIS objects which fall on the 'AGN area' of our classification system (Section 4.1). The [6.7/15] ratio alone does not separate them from late-type galaxies. Those of the QSO potentials which have a LW3 detection only are also likely candidates for type 2 Seyfert galaxies, which seem to have a suppressed 6–12 μm continuum (Spinoglio et al. 1995). Overall, QSOs have quite a large range of spectral shapes in the mid-IR (Haas et al. 2000), making detailed predictions difficult.

The reddest source in Fig. 7 has $J-K\approx 2.5$, which would qualify it as an extremely red object (ERO) candidate (e.g. Cimatti et al. 1999; Scodeggio & Silva 2000; Pozzetti & Mannucci 2000) – it does not have any optical counterpart to the POSS limits, making it at least $R-K>5$. It has only a LW3 detection, but this is due to lacking coverage with LW2. Thus far EROs have been selected and studied in the optical and near-IR, and there is an interesting degeneracy in explaining their nature: their colours could signify either an old elliptical at $z>1$, or a young, dusty star-forming galaxy. According to the GRASIL models, an elliptical would have $J-K\sim 2.5$ at $z>2$. Ellipticals, especially distant ones, would not have been seen by the ELAIS survey, and in any case the low $[2.2/15]\approx 0.1$ colour shows the presence of significant dust emission. Thus, the mid-IR can break the degeneracy of ERO observations. A detailed search for red objects using deeper optical imaging and our near-IR data, accompanied with the mid-IR *ISO* data, is thus of high importance.

5 CONCLUSIONS

We have presented photometry of a subsample of the ELAIS ISOCAM survey from the N1 and N2 fields. Our near-IR survey reaches down to $J\approx 19$ and $K\approx 17.5$. All of the 6.7 μm (LW2) REL = 2 sources are identified to these limits, as well as 84 per cent of 15 μm (LW3) REL = 2 sources. The detection efficiencies for REL = 3 sources are 88 and 35 per cent at LW2 and LW3 bands, respectively.

The near- and mid-IR stars were used, along with stellar models, to perform an accurate new calibration of the ELAIS ISOCAM data at both 6.7 and 15 μm.

Stars were separated from galaxies using near- to mid-IR colours. At 6.7 μm, 80 per cent of the identified ELAIS objects are stars. In contrast, at 15 μm, 80 per cent of the near-IR identified ELAIS sources are galaxies.

Only one-third of LW3 galaxies are also detected in LW2, while two-thirds of LW2 galaxies are seen in LW3. The mid-IR survey as a whole mainly detects late-type spiral galaxies and starbursts. The faintest population of these is missed by the LW2 filter. The few objects missed by the longer mid-IR filter are most probably early-type galaxies. Simple arguments indicate that typical redshifts of the sample seen with both mid-IR bands are $z\leqslant 0.2$.

We have presented several colour–colour plots useful in studying the relative emission strengths of stellar, PAH and warm dust components in galaxies, and we discuss galaxy classification and star formation properties using the diagrams. In a [15/2.2] versus [6.7/2.2] plot the Hubble type of a galaxy can be roughly estimated from its position along the diagonal ($[6.7/15]=1$), which is a measure of the proportion of ISM in the galaxy. Of the near-IR identified galaxies detected with both mid-IR filters, 75 per cent fall in the Scd group. However, some of these might be earlier morphological types with significant nuclear star formation.

In the same [15/2.2] versus [6.7/2.2] plot the quiescent galaxies fall on the diagonal (where $[15/6.7]\approx 1$) with increasing star formation activity raising the galaxies above the one-to-one curve. The ELAIS galaxies are found to have significant star formation, as indicated by the [6.7/15] tracer ($f_\nu(6.7\ \mu\mathrm{m})/f_\nu(15\ \mu\mathrm{m})=0.67\pm 0.27$) as well as by estimates from published relations between mid-IR luminosity and SFR. Redshift information and resolved imaging are however needed to quantify SFRs better and to decide whether the

ELAIS galaxies are powered by strong nuclear starbursts or otherwise high star formation activity in the disc.

In quiescent galaxies, as indicated by their [60/100] *IRAS* colour, [6.7/15] remains very constant. These are also the galaxies where the classification of galaxies using near-IR/mid-IR ratios works the best. The mid-IR ratio starts to drop at hotter [60/100]. Using near-IR/mid-IR colours we find support for the view that both the increase of 15-μm emission and an apparent depletion of emission at 6.7 μm are responsible for the effect. At these higher [60/100] levels, both [6.7/15] and [2.2/15] ratios (anti) correlate well with the [60/100] activity level indicator, thus making them useful tracers of star formation.

The ELAIS survey covered here detects several active galactic nuclei. By selecting objects using a 'KX method' (considering optical to near-IR properties only) we pick out sources from our catalogue whose mid-IR fluxes are consistent with the objects being AGN/QSOs.

ACKNOWLEDGMENTS

We wish to thank Kalevi Mattila for very useful discussions and suggestions, and an anonymous referee for thoughtful and valuable criticism. We thank A. Boselli for providing his mid-IR fluxes. This research has made use of the NASA/IPAC Extragalactic Database (NED), which is operated by the Jet Propulsion Laboratory, California Institute of Technology, under contract with the National Aeronautics and Space Administration. This publication makes use of data products from the Two Micron All Sky Survey (2MASS), which is a joint project of the University of Massachusetts and the Infrared Processing and Analysis Centre/California Institute of Technology, funded by the National Aeronautics and Space Administration and the National Science Foundation. This research has made use of the APS Catalog of POSS I, which is supported by the National Aeronautics and Space Administration and the University of Minnesota. The APS data bases can be accessed at http://aps.umn.edu/.

REFERENCES

Aussel A., Cesarsky C. J., Elbaz D., Starck J. L., 1999, A&A, 342, 313
Barkhouse W. A., Hall P. B., 2001, AJ, 121, 2843
Bertin E., Arnouts S., 1996, A&AS, 117, 393
Blommaert J. A. D. L., Siebenmorgen R., Coulais A., Okumura K., Ott S., Sauvage M., Starck J.-L., 2001, The ISO Handbook Volume III: CAM – The ISO Camera, http://www.iso.vilspa.esa.es/
Boselli A. et al., 1998, A&A, 335, 53
Cesarsky C. J., Sauvage M., 1999, Ap&SS, 269, 303
Cesarsky D., Lequeux J., Abergel A., Perault M., Palazzi E., Madden S., Tran D., 1996, A&A, 315, L309
Ciliegi P. et al., 1999, MNRAS, 302, 222
Cimatti A. et al., 1999, A&A, 352, L45
Crampton D., Janson T., Durrell P., Cowley A. P., Schmidtke P. C., 1988, AJ, 96, 816
Cutri R. M. et al., 2000, Explanatory Supplement to the 2MASS Second Incremental Data Release, http://www.ipac.caltech.edu/2mass/releases/second/doc/explsup.html
Dale D. A., Helou G., Silbermann N. A., Contursi A., Malhotra S., Rubin R. H., 1999, AJ, 118, 2055
Dale D. A. et al., 2000, AJ, 120, 583
Efstathiou A. et al., 2000, MNRAS, 319, 1169
Elbaz D. et al., 1999a, A&A, 351, L37
Elbaz D. et al., 1999b, in Cox P., Kessler M. F., eds, ESA SP-47, The Universe as Seen by ISO. ESA Publ. Div., ESTEC, Noordwijk, p. 999
Flores H. et al., 1999, ApJ, 517, 148
Francis P. J., Whiting M. T., Webster R. L., 2000, PASA, 17, 56
Genzel R., Cesarsky C. J., 2000, ARA&A, 38, 761
Haas M., Müller S. A. H., Chini R., Meisenheimer K., Klaas U., Lemke D., Kreysa E., Camenzind M., 2000, A&A, 354, 453
Helou G., 1986, ApJ, 311, L33
Helou G., 1999, in Cox P., Kessler M. F., eds, ESA SP-47, The Universe as Seen by ISO. ESA Publ. Div., ESTEC, Noordwijk, p. 797
Helou G., 2000, in Casoli F., Lequeux J., David F., eds, Les Houches Session LXX, Infrared Space Astronomy, Today and Tomorrow. EDP Sciences, Springer, Berlin, p. 337
Helou G., Lu N. Y., Werner M. W., Malhotra S., Silbermann N., 2000, ApJ, 532, L21
Kauffmann G., Charlot S., 1998, MNRAS, 297, L23
Kennicutt R. C., 1998, ARA&A, 36, 189
Lari C. et al., 2001, MNRAS, 325, 1173
Laurent O., Mirabel I. F., Charmandaris V., Gallais P., Madden S. C., Sauvage M., Vigroux L., Cesarsky C., 2000, A&A, 359, 887
Léger A., Puget J. L., 1984, A&A, 137, L5
Madden S. C., Vigroux L., Sauvage M., 1999, in Cox P., Kessler M. F., eds, ESA SP-47, The Universe as Seen by ISO. ESA Publ. Div., ESTEC, Noordwijk, p. 933
Mattila K., Lehtinen K., Lemke D., 1999, A&A, 342, 643
Missoulis V., Crockett H., Oliver S., Dapergolas A., Serjeant S., Rowan-Robinson M., Kontizas E., Kontizas M., 1999, in Cox P., Kessler M. F., eds, ESA SP-47, The Universe as Seen by ISO. ESA Publ. Div., ESTEC, Noordwijk, p. 85
Morel T. et al., 2001, MNRAS, 327, 1187
Oliver S. et al., 1997, MNRAS, 289, 471
Oliver S. et al., 2000, MNRAS, 316, 749
Pennington R. L., Humphreys R. M., Odewahn S. C., Zumach W., Thurmes P. M., 1993, PASP, 105, 521
Pozzetti L., Mannucci F., 2000, MNRAS, 317, L17
Roche P. F., Aitken D. K., Smith C. H., James S. D., 1986, MNRAS, 218, 19
Roussel H. et al., 2001a, A&A, 369, 473
Roussel H., Sauvage M., Vigroux L., Bosma A., 2001b, A&A, 372, 427
Roussel H. et al., 2001, A&A, 372, 406
Rowan-Robinson M. et al., 1999, in Cox P., Kessler M. F., eds, ESA SP-47, The Universe as Seen by ISO. ESA Publ. Div., ESTEC, Noordwijk, p. 1011
Sauvage M., Thuan T. X., 1994, ApJ, 429, 153
Sauvage M. et al., 1996, A&A, 315, L89
Schmitt H. R., Kinney A. L., Calzetti D., Storchi-Bergmann T., 1997, AJ, 114, 592
Scodeggio M., Silva D. R., 2000, A&A, 359, 953
Serjeant S. et al., 2000, MNRAS, 316, 768
Silva L., Granato G. L., Bressan A., Danese L., 1998, ApJ, 509, 103
Songaila A., Cowie L. L., Hu E. M., Gardner J. P., 1994, ApJS, 94, 461
Spinoglio L., Malkan M. A., Rush B., Carrasco L., Recillas-Cruz E., 1995, ApJ, 453, 616
Spoon H. W. W., Keane J. V., Tielens A. G. G. M., Lutz D., Moorwood A. F. M., 2001, A&A, 365, L353
Taniguchi Y. et al., 1997, A&A, 328, L9
Väisänen P., Tollestrup E. V., Willner S. P., Cohen M., 2000, ApJ, 540, 593
Vigroux L. et al., 1996, A&A, 315, L93
Vigroux L. et al., 1999, in Cox P., Kessler M. F., eds, ESA SP-47, The Universe as Seen by ISO. ESA Publ. Div., ESTEC, Noordwijk, p. 805
Warren S. J., Hewett P. C., Foltz C. B., 2000, MNRAS, 312, 827
Xu C., 2000, ApJ, 541, 134

APPENDIX A: CALIBRATION OF ISOCAM FLUXES USING INFRARED STARS

The ELAIS catalogue v.1.3 uses a one-to-one conversion of ADUs $\mathrm{gain}^{-1}\ \mathrm{s}^{-1}$ to mJy fluxes. The ISOCAM handbook values are 2.32 and 1.96 ADU $\mathrm{gain}^{-1}\ \mathrm{s}^{-1}\ \mathrm{mJy}^{-1}$ for the 6.7 and 15 μm filters, respectively (Blommaert 1998) – the reason for a factor of ∼2 difference is the lack of source stabilization correction in ELAIS data

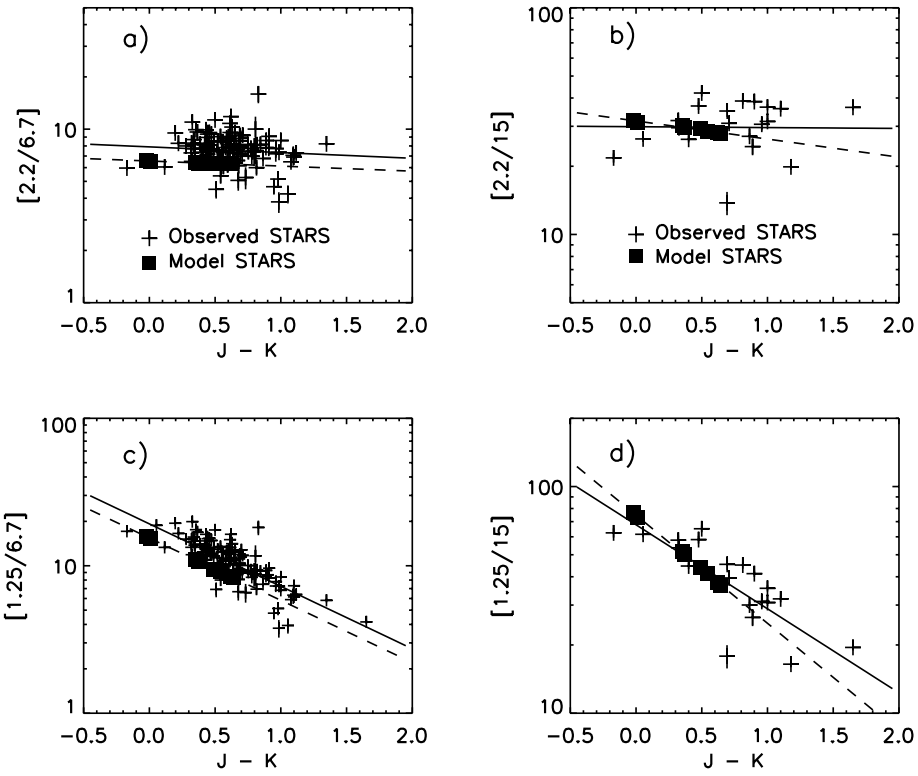

Figure A1. Stars in near-IR/mid-IR versus $J-K$ diagram. The 6.7 and 15 μm fluxes of the ELAIS v.1.3 catalogue stars (crosses) have been converted assuming 1 ADU gain^{-1} s^{-1} mJy^{-1}. The K-band flux uses $f_K = 6.20 \times 10^5 \times 10^{-0.4K}$ mJy and the J-band flux uses $f_J = 1.52 \times 10^6 \times 10^{-0.4J}$ mJy. The model colours (filled squares) have been calculated from several stellar spectra templates used in the ISOCAM calibration programme. The stars range from A0 to K3 in spectral type, including giants and main-sequence stars. The reddest of our observed stars in $J-K$ would be expected to be M stars. The solid and dashed lines are fits to the observed data and model points, respectively. From these we derive a constant correction factor of 1.22 to the 6.7-μm fluxes (i.e. 1.22 ADU gain^{-1} s^{-1} mJy^{-1}) in panel (a). From panel (b) the conversion of 15-μm flux becomes 1.05 ADU gain^{-1} s^{-1} mJy^{-1}. Panels (c) and (d) show the fits using J-band magnitudes, instead of K, and the flux calibrations become 1.24 and 1.06 ADU gain^{-1} s^{-1} mJy^{-1} for the LW2 and LW3 filters, respectively.

as detailed in Serjeant et al. (2000) [see also Blommaert (1998) – it is noted therein that the stabilization correction remains the largest single uncertainty in ISOCAM flux calibration]. In other words, starting from the handbook value of ∼2 ADU gain^{-1} s^{-1} mJy^{-1} and correcting for the loss of flux resulting from lack of stabilization, the conversion becomes ∼1 ADU gain^{-1} s^{-1} mJy^{-1}.

However, in case of the LW3 data (Serjeant et al. 2000) find a discrepancy of a factor of 1.75 after a cross-correlation with 22 bright stars in the ELAIS fields – in that paper all 15 μm fluxes are thus multiplied by a factor of 2. The publicly available v.1.4 ELAIS catalogue uses the factor of 1.75 in 15-μm fluxes. In Missoulis et al. (1999) mid-IR fluxes were derived for the same stars using *B*- and *V*-band bolometric magnitudes from *Hipparcos* and SIMBAD, along with blackbody approximations. Correlating with observed fluxes, sensitivity factors of 0.56 and 0.70 ADU gain^{-1} s^{-1} mJy^{-1} were obtained for 6.7 and 15 μm, respectively.

With good-quality near-IR data, rather than optical data, we potentially have a better chance of deriving the calibration factor for ELAIS data using the stars in our survey area. We would greatly reduce the uncertainty of extrapolating the optical magnitudes into mid-IR, as well as the required precision in the spectral types of stars.

To compare with observations, we make use of observationally based stellar spectra used for the extensive ISOCAM and ISOPHOT calibration programs.[3] We calculated near- and mid-IR colours of stars with a range of spectral types from these spectra. The models are estimated to be accurate within 5 per cent. In the mid-IR the fluxes were colour-corrected (maximally a 7 per cent effect) following the convention of *ISO* fluxes which are determined using a constant energy spectrum (note that for LW3 the 'reference wavelength' is 14.3 μm).

From our own sample of stars, defined in Section 2.5, we use only those with the REL = 2 status. In addition, we exclude stars which have $K < 8$ mag, because of probable saturation in our near-IR images. Fig. A1(a) shows the stars detected at 6.7 μm plotted as [2.2/6.7] versus $J-K$, with the model stars overplotted as solid symbols. From the model points one can notice a slight colour term, where the later spectral types with redder $J-K$ have slightly lower [2.2/6.7]. Ignoring the negligible colour term, from the average difference of [2.2/6.7] ratios of observations and models, we derive a correction of 1.22 to the 6.7 μm fluxes of the v.1.3 ELAIS catalogue. Fig. A1(b) shows the equivalent plot for the 15 μm stars – there are far fewer stars here, but the overall calibration of the v.1.3 ELAIS catalogue seems quite accurate. We derive a 1.05 ADU gain^{-1} s^{-1} mJy^{-1} calibration for the LW3 data. Specifically, we do *not* find evidence for the factor of 2 (or 1.75) scaling used in Serjeant et al. (2000). Since we are using the same ELAIS data, from the same reduction process and the same photometric aperture corrections, the discrepancy has to come from the adopted method of extrapolating near-IR (our case) or optical magnitudes to the mid-IR. The *J*-band data can be used as well: panels (c) and (d) show the equivalent colour–colour plots with *J* flux. The calibration factors are

[3] See http://www.iso.vilspa.esa.es/users/expl_lib/ISO/wwwcal/cam.html/

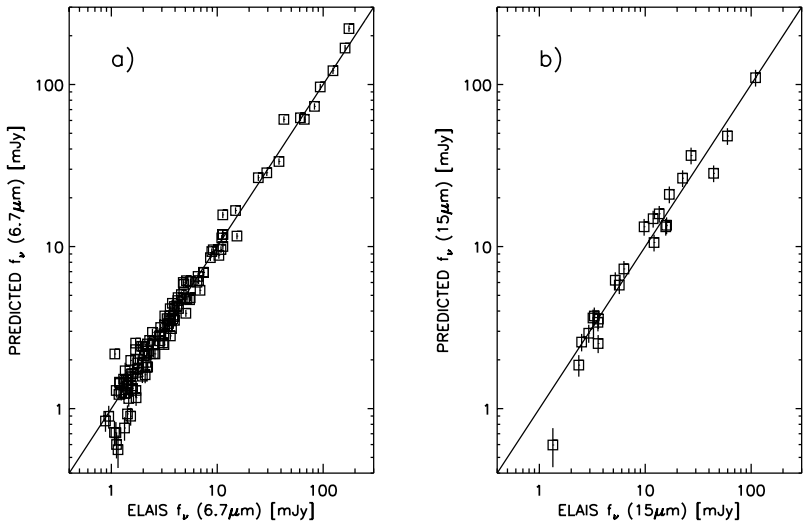

Figure A2. Predicted stellar fluxes versus the observed ELAIS fluxes. Panel (a) is for stars at 6.7 μm and (b) for the 15-μm stars. The predicted flux derivation uses *K*-band fluxes of stars and the [2.2/6.7] or the [2.2/15] ratio found from stellar models. The observed fluxes in (a) and (b) have been calibrated using the (small) differences (factors of 1.22 and 1.05, respectively) between the model and observed ratios (see the top panels of Fig. A1).

confirmed, as we find 1.24 and 1.06 ADU gain^{-1} s^{-1} mJy^{-1} for the LW2 and LW3 filters, respectively.

To compare with figures in Missoulis et al. (1999) and Serjeant et al. (2000), Fig. A2 shows the *predicted* 6.7 and 15 μm stellar fluxes (derived from the observed *K* magnitude of the star using the corresponding model colour ratio) against the observed and re-calibrated ELAIS 6.7 and 15 μm fluxes. The scatter is seen to be very small, and the relation highly linear over two orders of magnitude. We are thus confident of an accurate calibration for the ELAIS ISOCAM data.

In summary, in this paper we use the catalogue v.1.3 values for LW2 and LW3 multiplied by 1.23 and 1.05, respectively, to have the values in mJy (averages from *K* and *J* determination taken). The correction to conversion for LW3 is, in fact, smaller than the uncertainties related to the observed spread in mid-IR fluxes and the models, but we use it for consistency. Note that the v.1.4 ELAIS catalogue has the LW3 fluxes multiplied by 1.75, which needs to be taken into account if compared with results and plots in this paper.

This paper has been typeset from a TEX/LATEX file prepared by the author.